

# Integration, testing, and laboratory characterization of the mid-high layer wavefront sensor for LINC-NIRVANA

Matteo Lombini<sup>\*a,b</sup>, Italo Foppiani<sup>a,b</sup>, Emiliano Diolaiti<sup>a</sup>, Jacopo Farinato<sup>b,c</sup>, Roberto Ragazzoni<sup>c</sup>, Giovanni Bregoli<sup>a</sup>, Costantino Ciattaglia<sup>a</sup>, Giuseppe Cosentino<sup>d</sup>, Giancarlo Innocenti<sup>a</sup>, Laura Schreiber<sup>d</sup>, Carmelo Arcidiacono<sup>b,c</sup>, Fulvio De Bonis<sup>e</sup>, Sebastian Egner<sup>e</sup>, Wolfgang Gaessler<sup>e</sup>, Tom Herbst<sup>e</sup>, Martin Kuerster<sup>e</sup>, Johannes Schmidt<sup>e</sup>, Roberto Soci<sup>e</sup>, Pierfrancesco Rossettini<sup>f</sup>, Raffaele Tomelleri<sup>f</sup>

<sup>a</sup>INAF-Osservatorio Astronomico di Bologna, Via Ranzani 1, I-40127 Bologna, Italy

<sup>b</sup>INAF-Osservatorio Astrofisico di Arcetri, Largo Enrico Fermi 5, I-50125 Firenze, Italy

<sup>c</sup>INAF-Osservatorio Astronomico di Padova, Vicolo dell'Osservatorio 2, I-35122 Padova, Italy

<sup>d</sup>Università degli Studi di Bologna, Dipartimento di Astronomia, Via Ranzani 1, I-40127 Bologna, Italy

<sup>e</sup>Max Planck Institut fuer Astronomie, Koeningstuhl 17, D-69117 Heidelberg, Germany

<sup>f</sup>Tomelleri s.r.l., Via del Lavoro 25/a, I-37069 Villafranca, Verona, Italy

## ABSTRACT

The Mid-High Wavefront Sensors (MHWS) are components of the adaptive optics system of LINC-NIRVANA, the Fizeau interferometer that will be mounted at the LBT. These sensors, one for each telescope arm, will measure the atmospheric turbulence in the high altitude layers, using up to 8 reference stars in a 2 arcmin Field of View, and they will be coupled with two Ground Layer WFSs that will measure the lower part of the atmospheric turbulence using up to 12 stars over an annular Field of View from 2 to 6 arcmin in diameter. We will describe the opto-mechanical layout of the MHWS and the Assembly, Integration and Test (AIT) phase of the first sensor in the laboratory of the Bologna Observatory.

Keywords: Adaptive optics, Interferometry, High resolution, LBT

## 1. NIRVANA OVERALL DESCRIPTION

LINC-Nirvana is the Fizeau interferometer for LBT. In both arms of the telescope an MCAO module corrects the atmospheric turbulence. Before combining the beams a fringe tracker system removes the Optical Path Difference (OPD) through a piston mirror in order to create onto the scientific camera, operating in the near infrared, an interferometric image with a maximum spatial resolution corresponding to a 23m baseline. The wave front sensing in each arm is done by two sensors based on the multiple field of view layer-oriented approach<sup>5</sup>. One sensor, the Ground layer Wavefront Sensor (GWS), measures the ground layer turbulence of the atmosphere and can use up to 12 Reference Stars (RS) in an annular Field of View (FoV) from 2 to 6 arcmin. The Mid-High Wavefront Sensor (MHWS) measures the turbulence in the high layers of the atmosphere, using up to 8 RSs<sup>4</sup> in a circular FoV of 2 arcmin. The wavefront information measured by the GWFs is used to drive the two Adaptive Secondary mirrors of LBT while each of the two MHWSs drives a Deformable Mirror (DM) (with a provisional extension to two DMs per arm) mounted over the LINC-NIRVANA bench. After the adaptive optics correction, the light coming from the two arms is combined in the focal plane. To correct the Optical Path Difference (OPD) between the two beams, a Fringe Flexure Tracker (FFT) is used. A camera measures the fringe contrast of a star image inside a 1 arcmin FoV and this measurement is used to drive a piston mirror that corrects the OPD in real time. The infrared light (J, H, K bands) in the central 10 arcsec FoV is focused on the science focal plane, characterized by a fixed plate scale, allowing Nyquist sampling of the interferometric J band Point Spread Function (PSF).

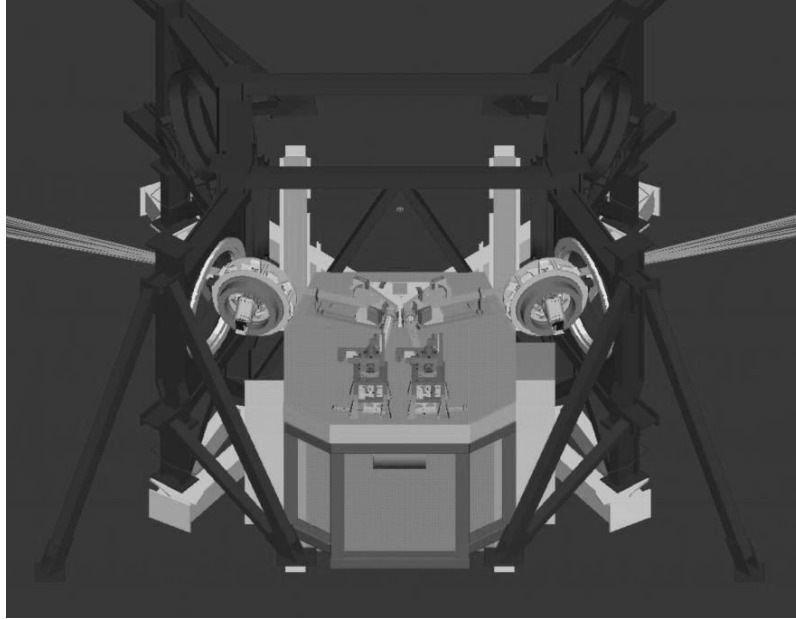


figure 1: Overall view of LINC-NIRVANA.

## 2. THE MID-HIGH WAVE FRONT SENSOR

The F/20 beam coming from the telescope is folded into the sensor by a mirror at 45 degrees and focused on a plane close to the Star Enlargers (SE), that are essentially formed by a couple of lenses having different focal length with the purpose of producing a magnified RS image on a pyramid prism. Each SE is positioned to pick the light of a RS by a couple of motorized Linear Stages (LS) arranged in an orthogonal way. The FoV is divided in four quadrants, each covered by two SEs. The images of the RSs used for wavefront sensing are separately magnified by the star enlargers and then the light is split in four parts by the pyramids. The four pupils coming from each RS are re-imaged by an objective and optically superimposed on a CCD conjugated to a certain height. The superimposition follows the geometry of the footprints of the stars at the conjugation height and depends on the angular separation among the stars and on the height of conjugation, the separation among the pupils increasing proportionally with these two parameters. In the initial configuration the MHWS will work with a single layer conjugation, but it is designed to work simultaneously with two conjugated layers, by placing a beam splitter that divides the light beam in two parts, forming distinct pupil images onto two CCDs conjugated to two different heights and coupled to two DMs. An overall view of the MHWS is shown in figure 1.

A known problem of the layer-oriented approach is the size of the re-imaged pupils, which imposes the use of large detectors with massive binning. This trouble is overcome in the MHWS by enlarging the focal ratio of each star individually rather than collectively, by means of the SE solution. In this way the pupil size, which is inversely proportional to the focal ratio, can be reduced, while the separation between the various stars across the FoV is left unchanged. Practical limits on the shrinking factor are imposed, for instance, by diffraction effects, which blur the re-imaged pupils<sup>10</sup>. The optical layout is shown in figure 3. The input of the MHWS is represented by the F/20 telecentric focal plane. The beam of each reference star, with focal ratio  $F$ , is collimated by a lens of focal length  $f_1$ , the first lens of the SE assembly, producing a small pupil image. The second lens of the SE, of focal length  $f_2$ , placed a distance  $f_2$  to the right of the intermediate pupil in order to preserve telecentricity, forms an enlarged image of the reference star with an equivalent focal ratio  $F' = kF$  where the enlarging factor is given by  $k = f_2/f_1$ . At this position, a pyramid is placed in order to split the light into four beams, which are focused by an objective of focal length  $f$  onto four pupil images. The re-imaged pupils corresponding to different RSs are collected by the objective (or two objectives if the beam splitter is inserted), which optically co-adds the light of the stars. The size of each re-imaged pupil is  $s = f/F'$ .

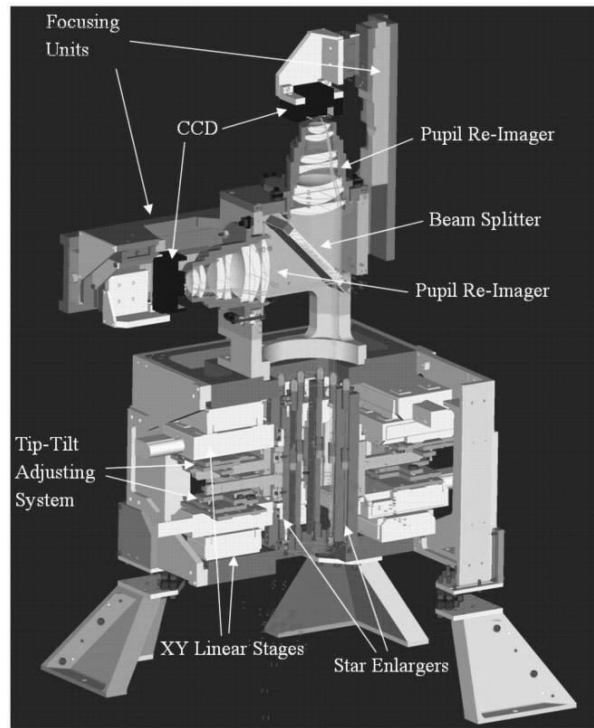


figure 2: A section of a 3D image of the MHWS, the “oil tower”.

The main requirements of the MHWS design are listed in table 1.

Item	Requirement
Input focal plane	F/20, telecentric, flat
Input FoV	2'
Working wavelength range	0.6 – 0.9 $\mu\text{m}$
Short wavelengths intensity attenuation	$< 10^{-2}$
Maximum number of reference stars	8
Minimum distance between two reference stars	Possibly $\leq 20''$
Conjugation range	4km – 15km (possible extension to 0 km)
Maximum (meta)pupil sampling	$21 \times 21$
Number of conjugated layers	2
Star Enlarger FoV	$\geq 1''$

table 1: Basic requirements and constraints on the MHWS design.

The choice of the SE magnifying factor  $k = 11.25$  and of the pupil re-imager focal length  $f = 99$  mm derives from the pupil diameter, imposed by the requirement to fit the meta-pupil of the 2 arcmin FoV at the maximum conjugation altitude (15 km) onto a quadrant of the available detector (EEV CCD39,  $80 \times 80$  pixel, pixel size  $24 \mu\text{m}$ ).

The main features of the MHWS components are described in the following.

### Pyramids

The pyramids are made of BK7 glass; the divergence angle  $\beta = 0.786^\circ$  corresponds to a vertex angle  $\alpha = 1.535^\circ$ , as defined in figure 6a. Considering the glass chromatic dispersion in the wavelength range of interest, the blur introduced by the pyramids on the pupil images amounts to approximately 10  $\mu\text{m}$  Peak-to-Valley (PtoV). The RMS blur is approximately 2.5 times smaller than the PtoV blur.

### Star enlargers

The star enlargers include two cemented doublets each, arranged in the configuration shown in figure 5. The first doublet has focal length  $f_1 = 14\text{mm}$  and diameter  $d_1 = 6\text{mm}$ ; the second doublet has focal length  $f_2 = 157.5\text{mm}$  and diameter  $d_2 = 12.7\text{mm}$ . The star enlargers have the purpose to increase independently the reference star linear dimensions leaving unchanged their mutual distance. In this way the pupil size, that is inversely related to the focal ratio, can be reduced to fit the CCD.

### Linear stages

The selection of a maximum of 8 references will be performed by 8 pairs of XY stages (LSs) for a total of 16 motorized linear stages per MHWS. As shown in figure 2, four XY stages will be mounted on the base plate of the main structure, while the other four will be mounted upside-down on another plate kept at the right distance from the first one by using properly shaped columns. The LSs are custom made because of the need to control the roll (which is normally not specified for commercial stages) and have it below  $10''$  (as for the pitch). This is done in order to minimize the relative displacement of the pupils created by the 8 star enlargers on the CCD when selecting RSs around the FoV.

### Objectives

The pupil re-imager is a 7-lens objective. It has a clear aperture  $d = 112\text{ mm}$  and a focal length  $f = 99\text{ mm}$ ; the working focal ratio is therefore approximately F/0.88. The design has been optimized in the wavelength range  $0.6 - 0.9\text{ }\mu\text{m}$  with uniform weighting. The equivalent FoV has been adjusted in order to match the CCD diagonal. The geometric RMS spot radius is approximately  $\sigma \approx 5.3\text{ }\mu\text{m}$ .

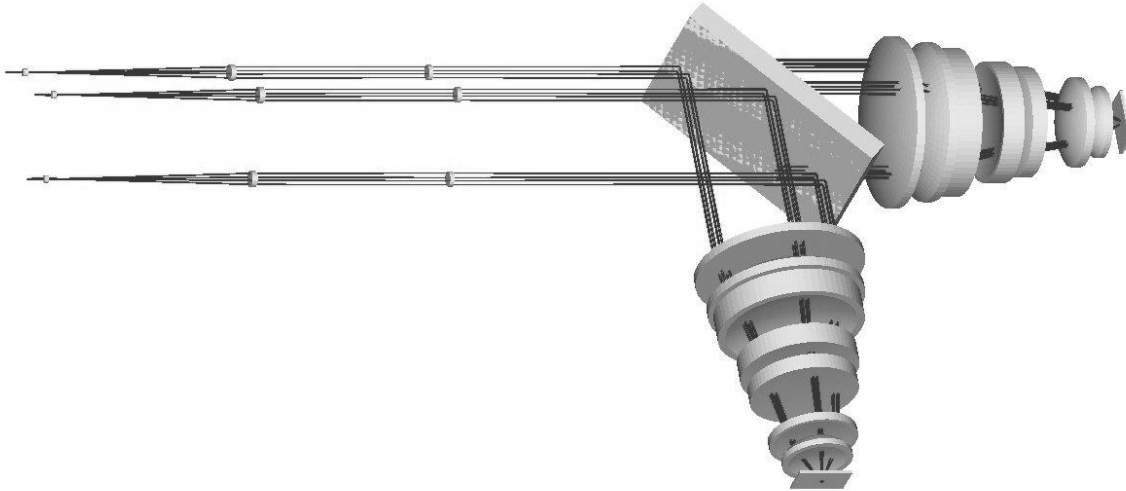


figure 3: Optical layout of the MHWS, 3 SEs are shown.

### 3. ASSEMBLY, INTEGRATION AND TESTS

The AIT of the two MHWFs will be done at the Bologna Observatory. All the components will be tested and mounted in the “oil tower”, as the MHWS is nicknamed. The main alignment tolerances are reported in table 2. The alignment specifications in general have been calculated in order to have a pupil blurring not larger than 1/10 of sub-aperture in the case of maximum CCD binning (21×21 sub-apertures), with the exception of the star enlarger focus (first tolerance in the table), which is related to the differential focus error of the various RSs and of the alignment tolerances of the pupil re-imager unit, coming from the tolerance analysis of that group.

Item	Tolerance
Star enlarger: distance FP20 – lens 1	±0.24 mm
Star enlarger distance lens 2 – pyramid	±30 mm
Star enlarger: distance lens 1 – lens 2	±0.1 mm
Star enlarger: relative centering lens 1 – lens 2	±0.1 mm (stability ±0.003 mm)
Star enlarger: pyramid centering	Astrometry requirement
Star enlarger tilt	Limited by pitch & roll of linear stages
Beam splitter tilt	±0.03° along major axis (±0.05° minor axis)
Pupil re-imager centering	±0.5 mm
Pupil re-imager tilt	±0.1°
CCD focus	±0.001 mm
CCD tilt	±1 mrad

table 2: Main alignment tolerances of the MHWS components.

#### Linear stages tests and assembly

The LS pitch and roll should be less than 10", in order to maintain the pupil displacement with respect to the theoretical position within 1/10 sub-aperture. Tests to check the performance of the LSs will be performed at MPIA in Heidelberg (Germany). The coupling of the LSs will be done in a way to fulfill the orthogonality of the movements of the two stages with an accuracy better than 1' (figure 4).

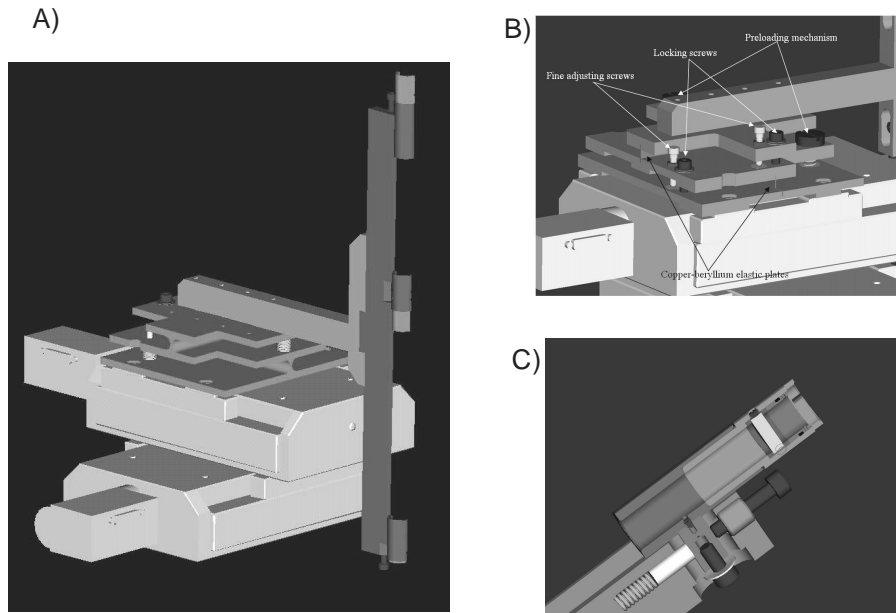


figure 4: a) a 3-D drawing of a star enlarger mounted over two linear stages in the orthogonal configuration; b) the tip-tilt mount of star enlargers; c) the pyramid barrel that can be adjusted in decenter and focus.

### Star Enlargers alignment and assembly

The enlarging factor  $k$  of the various SEs must be as similar as possible to avoid pupil blurring. According to the measurements provided by the lens manufacturing company (SILO, Italy), the focal lengths of the lenses of a given type are all within  $\pm 0.3\%$  from the average, which means an expected percentage error on the enlarging factor of order of  $\pm 0.5\%$ , corresponding to 1/10 sub-aperture pupil blur. The current plan is to couple the lenses and verify the enlarging factor of the SEs. As shown in figure 5, the SE is attached to a holder and aligned with respect to the collimated laser beam. Lens 2 focuses the beam at the entrance focus of the 6mm lens of the SE and Lens 1 produces an image of the entrance pupil (located before Lens 2) onto the CCD. Placing a mask with two holes of known separation in the entrance pupil plane, the distance between the two spots on the CCD provides a measurement of the enlarging factor of a given SE. Keeping the auxiliary lenses 1 and 2 in position, allows precise relative measurements of the enlarging factor of different SEs. After measuring the enlarging factor, we will align the SE lenses. They can be aligned in decenter and tilt and can be shifted along the optical axis. The alignment setup is based on the one shown in figure 5.

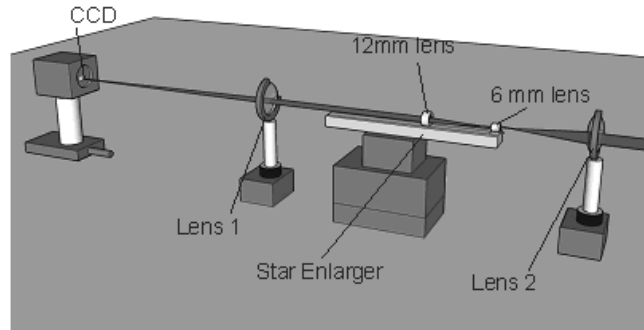


figure 5: A sketch of the set up for the measurement of the SE lenses magnifying factor.

### Pyramids measurements

The pyramids are placed in the focal plane formed by the two lenses of the SEs. The light of the RSs moves on the surroundings of the pyramid pin continuously because of the atmospheric turbulence, making the four pupils to change their mutual light intensity distribution. Sharp edges are needed to avoid light losses. Furthermore the vertex angle, calculated in order to make the pupils fit the CCD, must be very similar among all the SEs, in order to avoid a blurring of the pupil images. The measurement of the pyramids vertex angle is done by placing the pyramid along a collimated beam. The four beams produced by the pyramid interfere and are seen on a camera as in figure 6b. The Fourier Transformation of that image permits to calculate the vertex angle with the requested precision<sup>2</sup>. In table 3 the vertex angles of all the pyramids of the two MHWSs (including spare ones) are listed. Note that all vertex angles are within the specification.

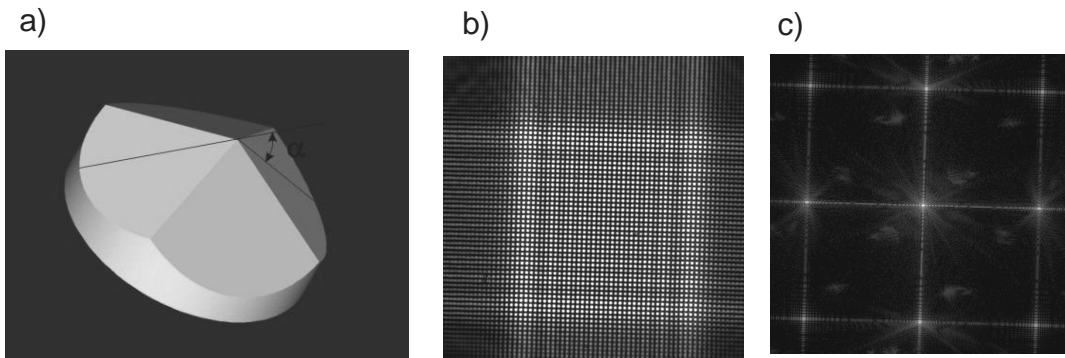


figure 6:a) a sketch of the pyramid. b) The image on the CCD when a collimated beam crosses the pyramid. c) The FFT image of the figure b, used to compute the divergence angle.

#	Angle 1-3	Angle 2-4	Mean angle	In spec
1	1.55633	1.55212	1.55422	√
2	1.55608	1.55231	1.55419	√
3	1.55349	1.55301	1.55325	√
5	1.55089	1.55063	1.55076	√
6	1.55249	1.55173	1.55211	√
7	1.55299	1.55256	1.55277	√
8	1.55189	1.54976	1.55082	√
9	1.55197	1.55006	1.55102	√
10	1.55035	1.55032	1.55033	√
11	1.55077	1.55056	1.55067	√
12	1.55247	1.55250	1.55248	√
13	1.55530	1.55370	1.55450	√
14	1.54866	1.55023	1.54945	√
15	1.54761	1.54828	1.54795	√
16	1.55577	1.55036	1.55307	√
17	1.54910	1.54967	1.54939	√
20	1.54739	1.54757	1.54748	√
21	1.54794	1.54617	1.54706	√
23	1.54900	1.55064	1.54982	√
24	1.55063	1.55016	1.55040	√
Mean			1.55109	√

**table 3: The mean value of all the pyramids vertex angle specification is  $1.55431^\circ \pm 0.0022^\circ$  while the vertex angle repeatability among the pyramids must be  $0.0044^\circ$  within the mean measured value.**

### Telescope simulator

The telescope simulator is used to check the MHWS performance. It simulates the F/20 telecentric beam at the entrance focus of the MHWS, allowing the open loop tests of the sensor using white light coming from a set of fibers and some plastic screens to simulate the atmospheric turbulent layers. In figure 7 there is a sketch of the telescope simulator setup. The lenses and the diaphragm are aligned with a laser checking the back reflected spots. The position of the lens L1 is defined by its focal length distance from the focal plane at the entrance of the MHWS, where it will be positioned on the NIRVANA bench. The positioning of the stop and of the lens L1 is accomplished by auto collimation: inserting a target at the stop position and placing a flat mirror after lens L1, we observe the back reflected spot focusing on the pupil plane when their mutual distance is equal to the focal length of L1. The same operation is done for the positioning of lens L2 with respect to the stop. Finally the auto collimation procedure is done also for the fiber plate. Once the components are properly aligned the light fibers are used for the alignment of the SEs and for the tests of the system performance. The light fibers (50µm core) are now seen by the MHWS as RSs.

### Star enlarger alignment and CCD focusing

Once the SEs are mounted in the MHWS structure, the pyramids will be placed on their top and will be aligned in rotation, so the wavefront measurements and the system characterization can be started. A different position of the SEs with respect to the entrance focal plane produces a differential defocus contribution on the wavefront of the various SEs, which can not be eliminated by calibration. The wavefront of the same on-axis RS will be measured positioning, once at a time, all the SEs over that star and the defocus aberration will be calculated. Taking into account the experience acquired with the LOWFS for MAD<sup>9</sup>, the whole structure of the SEs can be shifted along the optical path and be adjusted in order to null the possible static defocus term. The alignment in tip-tilt of the SEs is done by placing them off axis, at about 30 arcsec from the center of the FoV. This is because the pitch and roll of the LSs that produce a displacement of the pupils on the CCD must be averaged when the SEs are moved across the FoV.

The conjugation of the CCD to a given "altitude" in the simulated atmosphere is done by putting a mask with some holes at the corresponding height on the screen holder (figure 8). On the CCD four series of spots with the hole mask geometry will appear, formed by the pyramids. By placing various SEs on different off axis stars, we can find the proper conjugated position of the CCD as the position where the relative displacement of the spot images produced by the different stars is minimum.

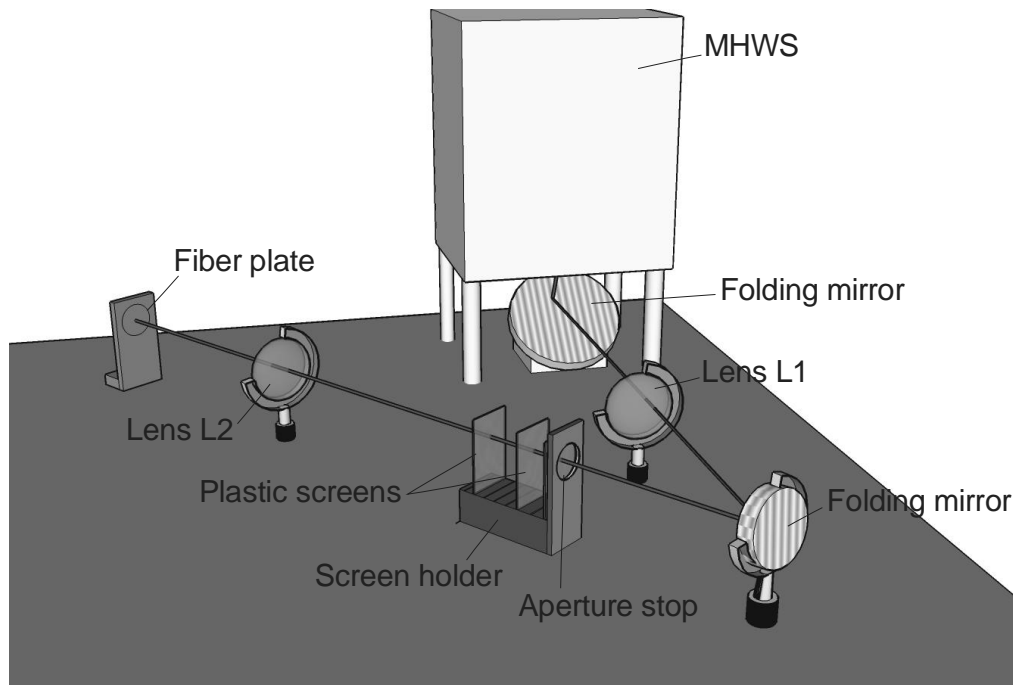


figure 7: A sketch of the Telescope simulator. The stop corresponds to the 8.2m telescope pupil aperture while the 50  $\mu\text{m}$  core light fibers placed at the fiber plate are seen by the pupil as RSs. The lens L1 focuses the beam at the entrance of the MHWS. Turbulence screens can be placed on the screen holder to simulate turbulence layers at different heights.

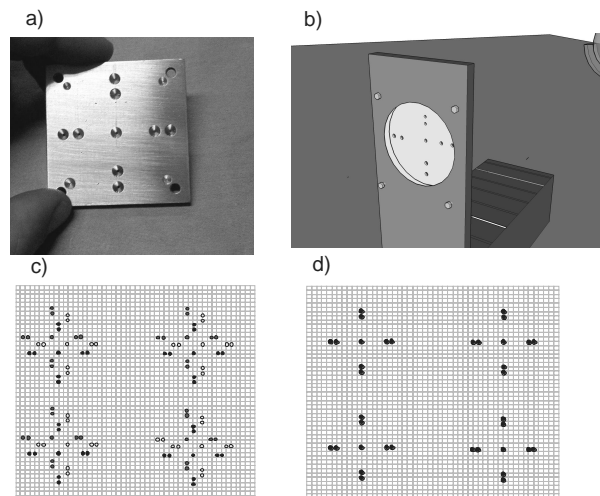
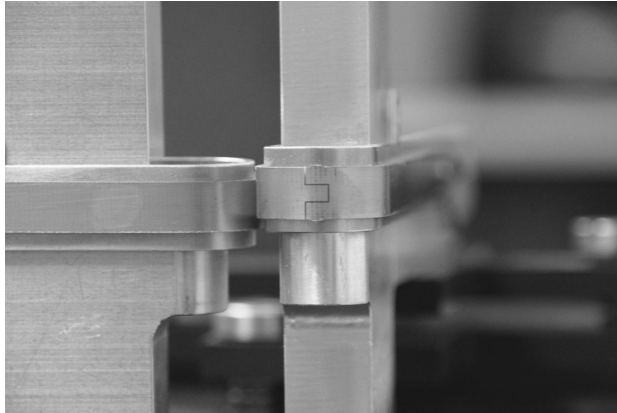


figure 8: a) The mask to be placed at the pupil to conjugate the CCD at that layer. b) A sketch of the mask mounted. c) The images of the mask produced by three off axis star enlargers when the CCD is not conjugated at the mask height. d) The same images at the right CCD conjugation.

### Collision control

To prevent major damages in case of failure of the LSs control software, a collision control hardware will be installed on the MHWS. Around the SE central lenses (figure 9) a copper strip will be attached and an electric wire at both sides of each strip will connect the SEs, which will shortcut and immediately will stop the stages run, as soon as a collision will occur. The copper strips will have a non-conductive gap at the top to determine which side the collision might happen.



**figure 9: picture of two star enlarger prototypes. Note the copper strips around the lens mounts.**

### Performance tests

Once the system will be aligned, several tests will be performed in order to verify the optical performance. Some plastic screens, characterized by an interferometer, will be placed at various positions of the screen holder to simulate turbulence layers of different height, following either the typical Mount Graham profile and different ones. One of the tests to perform is the turbulence measurement of a layer to which the CCD is conjugated, in order to check how the signal is degraded by the optics. For this reason the CCD will be conjugated to the ground layer, where the footprints of the various stars superimpose, and a plastic screen will be positioned close to the telescope simulator pupil, permitting the direct comparison of the measurements obtained with the interferometer and the MHWS. Then, the same test will be performed by conjugating the CCD at a high layer, where the footprints do not superimpose. Finally, several tests will be performed placing screens at different heights, to assess how accurately the MHWS measures the signal of layers to which it is not conjugated. Once the AIT will be completed, the MHWS will be shipped to Heidelberg to be integrated with the other components of NIRVANA and to be aligned and coupled with the DMs, in order to characterize the dynamic response of the system to a simulated turbulent atmosphere.

### ACKNOWLEDGMENT

Thanks to Flavio Fusi Pecci, Bruno Marano and Piero Salinari for their continuous support to this project.

### REFERENCES

1. Matteo Lombini, "Ottica adattiva a grande campo per il VLT", Degree Thesis, Università degli Studi di Bologna, 2003.
2. Arcidiacono C., "Beam divergence and vertex angle measurements for refractive pyramids", *Optics Communication*, 252, August 2005, pp 239-246 (2005).
3. Farinato J., Viard E., Ragazzoni R., Baruffolo A., Diolaiti E., Arcidiacono C., "Layer Oriented WSF Assembly Integration and test plan", ESO Doc. No.: OWL-PLA-INA – 60000-0065, Issue: 1.0.

4. Beckers J. M., "Increasing the size of the isoplanatic patch size with multiconjugate adaptive optics", in *ESO conference on Very Large Telescopes and their instrumentation*, M.-H. Hulrich, ed., pp. 693, 1988.
5. Ragazzoni R., Diolaiti E., Farinato J., Fedrigo E., Marchetti E., Tordi M., Kirkman D., "Multiple field of view layer-oriented adaptive optics. Nearly whole sky coverage on 8 m class telescopes and beyond", *A&A* 396, 731-744, 2002.
6. Ragazzoni R., "Pupil plane wave front sensing with an oscillating prism", *J. of Mod. Opt.* 43, pp. 289-293, 1996.
7. Ragazzoni R., Diolaiti E., Vernet E., Farinato J., Marchetti E., Arcidiacono C., "Arbitrarily small pupils in layer-oriented multi-conjugate adaptive optics", *PASP* 117, p. 860, 2005.
8. Bertram, T.; Straubmeier, C.; Rost, S.; Eckart, A., The Fringe and Flexure Tracking System for the LBT interferometric camera LINC-NIRVANA., *Astron. Nachr.*, 326, 560-561, 2005.
9. Soci R., Baumeister H., Rohloff R., Diolaiti E., Xu W., Andersen D., Egner S., Arcidiacono C., Lombini M., Ebert M., Boehm A., Muench N., Xompero M., "LINC-NIRVANA: mechanical challenges of the MCAO wavefront sensor", *Proceedings of the SPIE*, Volume 5490, pp. 1286-1295, 2004.